J Physiol 00.0 (2020) pp 1–16

The Journal of Physiology

Opposing modulation of Cx26 gap junctions and hemichannels by CO_2

Sarbjit Nijjar[1], Daniel Maddison[1], Louise Meigh[1], Elizabeth de Wolf[1], Thomas Rodgers[2], Martin J. Cann[3] and Nicholas Dale[1]

[1] *School of Life Sciences, University of Warwick, Coventry, UK*
[2] *School of Chemical Engineering and Analytical Science, University of Manchester, Manchester, UK*
[3] *Department of Biosciences, Durham University, Durham, UK*

Edited by: David Wyllie & Florian Lesage

Key points

- A moderate increase in P_{CO_2} (55 mmHg) closes Cx26 gap junctions.
- This effect of CO_2 is independent of changes in intra- or extracellular pH.
- The CO_2-dependent closing effect depends on the same residues (K125 and R104) that are required for the CO_2-dependent opening of Cx26 hemichannels.
- Pathological mutations of Cx26 abolish the CO_2-dependent closing of the gap junction.
- Elastic network modelling suggests that the effect of CO_2 on Cx26 hemichannels and gap junctions is mediated through changes in the lowest entropy state of the protein.

Abstract Cx26 hemichannels open in response to moderate elevations of CO_2 (P_{CO_2} 55 mmHg) via a carbamylation reaction that depends on residues K125 and R104. Here we investigate the action of CO_2 on Cx26 gap junctions. Using a dye transfer assay, we found that an elevated P_{CO_2} of 55 mmHg greatly delayed the permeation of a fluorescent glucose analogue (NBDG) between HeLa cells coupled by Cx26 gap junctions. However, the mutations K125R or R104A abolished this effect of CO_2. Whole cell recordings demonstrated that elevated CO_2 reduced the Cx26 gap junction conductance (median reduction 66.7%, 95% CI, 50.5–100.0%) but had no effect on $Cx26^{K125R}$ or Cx31 gap junctions. CO_2 can cause intracellular acidification. Using 30 mM propionate, we found that acidification in the absence of a change in P_{CO_2} caused a median reduction in the gap junction conductance of 41.7% (95% CI, 26.6–53.7%). This effect of propionate was unaffected by the K125R mutation (median reduction 48.1%, 95% CI, 28.0–86.3%). pH-dependent and CO_2-dependent closure of the gap junction are thus mechanistically independent. Mutations of Cx26 associated with the keratitis ichthyosis deafness syndrome (N14K, A40V and A88V), in combination with the mutation M151L, also abolished the CO_2-dependent gap junction closure.

Sarbjit Nijjar received a PhD in developmental biology from Kings College London. He then undertook postdoctoral research at the University of Warwick on the development of the embryonic kidney. Moving to the University of Birmingham, his research activities focused on the pathobiology of human liver disease. His current research in the laboratory of Prof. Nicholas Dale at the University of Warwick has focused on understanding the regulation, by carbon dioxide, of the membrane channel protein connexin 26. This has provided insights into how disruption of this regulatory mechanism may contribute to defects in diverse physiological processes such as breathing and hearing.

This paper was first published as a preprint: Nijjar S, Maddison D, Meigh L, de Wolf E, Rodgers T, Cann M, Dale N (2020). Opposing modulation of Cx26 gap junctions and hemichannels by CO_2. *bioRxiv*. https://doi.org/10.1101/584722.

DOI: 10.1113/JP280747

Elastic network modelling suggests that the lowest entropy state when CO_2 is bound is the closed configuration for the gap junction but the open state for the hemichannel. The opposing actions of CO_2 on Cx26 gap junctions and hemichannels thus depend on the same residues and presumed carbamylation reaction.

(Received 7 September 2020; accepted after revision 2 October 2020; first published online 6 October 2020)
Corresponding author N. Dale: School of Life Sciences, University of Warwick, Gibbet Hill Rd, Coventry CV4 7AL, UK. Email: n.e.dale@warwick.ac.uk

Introduction

The canonical function of connexins is to form intercellular junctions between cells – gap junctions – through the docking of hexameric connexons in the opposing membrane of each cell. However, the individual connexons – known as hemichannels – can also function on their own (Stout *et al.* 2004; Weissman *et al.* 2004; Pearson *et al.* 2005; Huckstepp *et al.* 2010*b*). Hemichannels act as plasma membrane channels, which, in addition to mediating transmembrane ionic currents, permit the transmembrane fluxes of small molecules such as ATP (Stout *et al.* 2002; Pearson *et al.* 2005; Kang *et al.* 2008; Huckstepp *et al.* 2010*a*).

By means of electrophysiological and dye-loading assays, we have studied the hemichannels of connexin26 (Cx26) and demonstrated that they are directly gated by CO_2 (Huckstepp *et al.* 2010*a*; Meigh *et al.* 2013, 2014). CO_2 opens the hemichannel and permits the efflux of ATP, which can act as a neurotransmitter. This is particularly important in the CO_2-sensitive control of breathing where Cx26 hemichannels in the medulla oblongata act as novel chemosensory transducers (Huckstepp *et al.* 2010*a*; Huckstepp & Dale, 2011). Cx26 hemichannels also impart CO_2 sensitivity to dopaminergic neurons of the substantia nigra and GABAergic neurons of the ventral tegmental area (Hill *et al.* 2020). The action of CO_2 on Cx26 has been proposed to occur via carbamylation of the residue K125 (Meigh *et al.* 2013). CO_2 carbamylation, sometimes called carboxylation, involves formation of a covalent bond between the nitrogen atom of a primary amine (in this case the lysine side chain) and the carbon atom of CO_2. The resulting carbamylated amine bears a negative charge distributed over the oxygen atoms (and essentially converts the lysine side chain from a basic to an acidic moiety). This reaction differs from carbamylation involving cyanate, which results in a very stable modification of the amine. Unlike this latter reaction, CO_2 carbamylation is a highly reversible post-translational modification (Lorimer, 1983; Meigh, 2015).

The carbamylated lysine forms a salt bridge to R104 of the neighbouring subunit. These intersubunit carbamate bridges bias the hemichannel to the open configuration (Meigh *et al.* 2013). Extensive evidence supports a direct action of CO_2 on the hemichannel rather than an indirect effect via pH: (1) in isolated inside-out or outside-out patches, changes in P_{CO_2} at constant pH alter Cx26-gating (Huckstepp *et al.* 2010*a*); (2) insertion of the carbamylation motif into Cx31, which is insensitive to CO_2, creates mutant Cx31 hemichannels that can be opened by CO_2 (Meigh *et al.* 2013); (3) mutation of the key residues K125 and R104 to respectively arginine and alanine destroys CO_2 sensitivity of the hemichannel; (4) the mutations K125E and R104E (in effect engineering the action of CO_2 into the subunit via the carboxy group of glutamate) create constitutively open hemichannels which are CO_2-insensitive (Meigh *et al.* 2013); (5) the mutation K125C creates a hemichannel that can be opened with NO or NO_2 via a nitrosylation reaction on the cysteine residue at position 125 and subsequent salt bridge formation to R104 (Meigh *et al.* 2015); and (6) the double mutation K125C and R104C creates a redox-sensitive hemichannel presumably via disulfide bridge formation between the cysteine residues at positions 104 and 125 (Meigh *et al.* 2015). Based on this understanding of how CO_2 modulates the Cx26, we have created a Cx26 subunit with the combined mutations K125R and R104A. This doubly mutated Cx26 subunit coassembles with wild-type Cx26 and removes sensitivity from the resulting heteromeric hexamer and therefore has a dominant negative action on the CO_2 sensitivity of wild-type Cx26 (van de Wiel *et al.* 2020). By expressing this doubly mutated subunit in glial cells of a confined target area of the medulla oblongata (the caudal parapyramidal area), we have demonstrated that CO_2 binding to Cx26 contributes about half of the adaptive ventilatory response to hypercapnia that is controlled by central chemosensors (van de Wiel *et al.* 2020). Cx26 also plays a role in mediating CO_2-dependent modulation of the excitability of neurons in the substantia nigra and ventral tegmental area (Hill *et al.* 2020). We have also recently demonstrated that K125 is indeed carbamylated and produced new high resolution cryoEM structures of Cx26 at different levels of P_{CO_2} (Brotherton *et al.* 2020). Thus, carbamylation of Cx26 occurs and is involved in mediating the CO_2-dependent control of physiologically important functions.

Although the actions of CO_2 on Cx26 hemichannels are well characterized, we have not studied the action of CO_2 on Cx26 gap junctions. When the two connexons dock to form a complete gap junction, there is likely to be significant conformational rearrangement and constraint

of the resulting dodecameric complex. Therefore, we cannot assume that CO_2 will modulate a complete gap junction in the same way as a hemichannel. There has been a previous study on the closing effect of CO_2 on Cx32 and Cx26 gap junctions expressed in *Xenopus* oocytes (Young & Peracchia, 2004). This prior study used non-physiological conditions in which both the extracellular and intracellular pH would become very acidic: exposure to 30–100% CO_2 in the absence of bicarbonate in the extracellular medium. This study most likely reported an effect of pH on the gap junction. In this paper, we report the actions of much lower physiological concentrations of CO_2 (~9%), in a CO_2/HCO_3^--buffered system at constant extracellular pH, on gap junctions formed between pairs of HeLa cells expressing Cx26. We find that modest increases in P_{CO_2} *close* complete gap junctions, and that this is most likely a direct effect mediated through CO_2 binding to the same residues that result in the *opening* of the hemichannel. This result reinforces the need to develop further high-resolution structures for Cx26 hemichannels and gap junctions with and without CO_2 bound.

Methods

HeLa cell culture and transfection

HeLa DH (ECACC) cells were grown in Dulbecco's modified Eagle's medium supplemented with 10% fetal bovine serum, 50 μg ml^{-1} penicillin–streptomycin and 3 mM $CaCl_2$. For electrophysiology and intercellular dye transfer experiments, cells were seeded onto coverslips in six-well plates at a density of 2×10^4 cells per well. After 24 h the cells were transiently transfected with Cx26 constructs tagged at the C-terminus with a fluorescent marker (mCherry) according to the GeneJuice Transfection Reagent protocol (Merck Life Science UK Limited, Gillingham, Dorset, UK). The HeLa cells stably expressing mouse Cx26 were originally obtained from Dr K. Willecke (Elfgang *et al.* 1995).

Cx26 mutants

The mutations used in this study were introduced into the Cx26 gene by QuikChange site directed mutagenesis and have been described previously (Meigh *et al.* 2013; Cook *et al.* 2019).

Solutions used

Standard artificial cerebrospinal fluid (aCSF): 124 mM NaCl, 3 mM KCl, 2 mM $CaCl_2$, 26 mM $NaHCO_3$, 1.25 mM NaH_2PO_4, 1 mM $MgSO_4$, 10 mM D-glucose saturated with 95% O_2–5% CO_2, pH 7.5, P_{CO_2} 35 mmHg. Hypercapnic aCSF: 100 mM NaCl, 3 mM KCl, 2 mM $CaCl_2$, 50 mM $NaHCO_3$, 1.25 mM NaH_2PO_4, 1 mM $MgSO_4$, 10 mM D-glucose, saturated with 9% CO_2 (with the balance being O_2) to give a pH of 7.5 and a P_{CO_2} of 55 mmHg. Propionate solution: 82 mM NaCl, 30 mM sodium propionate, 3 mM KCl, 2 mM $CaCl_2$, 26 mM $NaHCO_3$, 1.25 mM NaH_2PO_4, 1 mM $MgSO_4$, 10 mM D-glucose saturated with 95% O_2–5% CO_2, pH 7.5, P_{CO_2} 35 mmHg.

Imaging assay of gap junction transfer

2-Deoxy-2-[(7-nitro-2,1,3-benzoxadiazol-4-yl) amino]-D-glucose (NBDG) was included at 200 μM in the patch recording fluid, which contained: potassium gluconate 130 mM; KCl 10 mM; EGTA 5 mM; $CaCl_2$ 2 mM, Hepes 10 mM, pH adjusted to 7.3 with KOH and a resulting final osmolarity of 295 mOsm. Cells were imaged on a Cleverscope (MCI Neuroscience, Framfield, East Sussex, UK) with a Photometrics Prime camera under the control of Micromanager 1.4 software. LED illumination (Cairn Research, Faversham, UK) and an image splitter (Optosplit, Cairn Research) allowed simultaneous imaging of the mCherry-tagged Cx26 subunits and the diffusion of the NBDG into and between cells. Coupled cells for intercellular dye transfer experiments were initially selected on the basis of tagged Cx26 protein expression and the presence of a gap junctional plaque, easily visible as a band of mCherry fluorescence (e.g. Figs 1 and 2). After establishing the whole cell mode of recording, images were collected every 10 s.

Patch clamp recordings from coupled cells

Coverslips containing non-confluent cells were placed into a perfusion chamber at room temperature in sterile filtered standard aCSF. Two Axopatch 200B amplifiers (Molecular Devices, San Jose, CA, USA) were used to make whole-cell recordings from pairs of HeLa cells. The intracellular fluid in the patch pipettes contained: potassium gluconate 130 mM, KCl 10 mM, EGTA 10 mM, $CaCl_2$ 2 mM, Hepes 10 mM, sterile filtered, pH adjusted to 7.3 with KOH. An agarose salt bridge was used to avoid solution changes altering the potential of the Ag–AgCl reference electrode. All whole-cell recordings were performed at a holding potential of −50 mV. Steps to −40 mV were applied to each cell in alternation to measure the whole cell and gap junction conductances. A similar protocol has been previously used by others (Wang *et al.* 2003). The current from the cell at −40 mV to the cell at −50 mV flows through the gap junction and can thus be used to calculate the gap junction conductance. The outward current during the +10 mV step in each cell represents the whole cell conductance, which is a combination of all current pathways out of the cell. These comprise any intrinsic conductances and also the gap junction conductance itself.

Elastic network modelling

Elastic network model (ENM) simulations were performed based on the regular implementation using PDB file 2ZW3, where all the Cα atoms in the protein within a given cut-off radius (8 Å) were joined with simple Hookean springs (Tirion, 1996; Rodgers *et al.* 2013*a*). An 8 Å cut-off radius was selected based on previous observations for the optimal correlation value for B factors between the calculated ENM and a crystal structure (Townsend *et al.* 2015). The spring constants were set to a constant value of 1 kcal mol^{-1} Å^{-2}. The presence of CO_2 was represented in the ENM by the inclusion of an additional Hookean spring between residues K125 and R104 of each set of neighbouring monomers, following the same procedure previously used for ligand binding (Rodgers *et al.* 2013*b*). The mass-weighted second derivatives of this potential energy matrix were diagonalized to produce eigenvectors, *e*, which are the normal modes, and eigenvalues which, are the squares of the associated frequencies, ω, and can be used to calculate the free energy of each mode.

The first six modes, that is the lowest frequency modes, represent the solid body translational and rotational motions of the protein and are thus excluded from the analysis. The overlap of the modes in the unbound and CO_2-bound states were calculated by comparison of the eigenvectors (Rodgers *et al.* 2013*a*). A value of 1 indicates that the motions are identical whereas a value of 0 indicates that the motions are completely different.

Statistics and reproducibility

Statistical analysis was performed with the R language. Data have been plotted as box and whisker plots, with individual points superimposed, where the box is interquartile range, bar is median and whisker extends to most extreme data point that is no more than 1.5 times the interquartile range. Each individual point is from a single patch clamp experiment and is counted as a replicate. Statistical comparisons were performed with the Kruskal–Wallis test (for multiple comparisons) or Mann Whiney *U* test. Exact *P* values are shown for comparisons that showed a significant difference between samples.

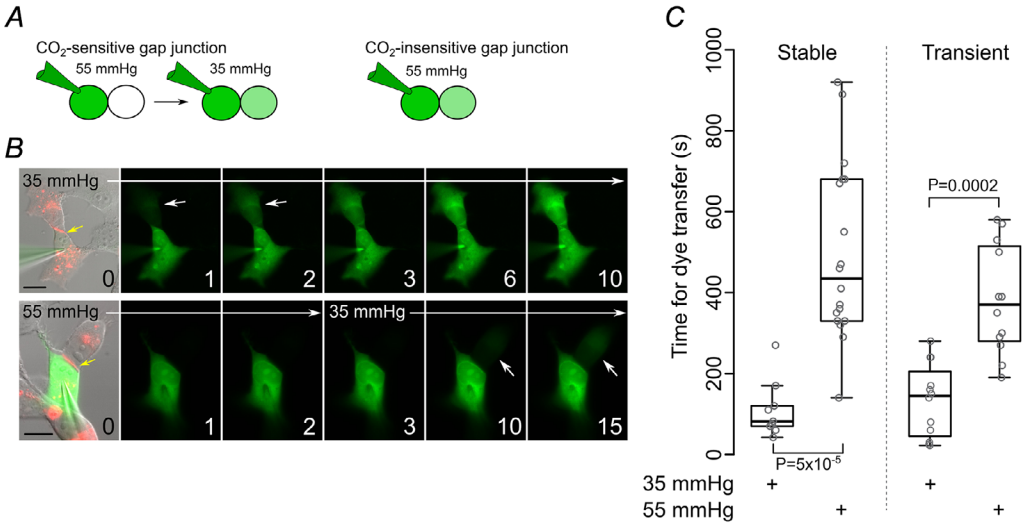

Figure 1. Dye transfer assay to assess the CO_2 sensitivity of gap junction coupling
A, logic of the assay: a CO_2-sensitive gap junction will display no or very little dye transfer from the donor to acceptor cell under conditions of high P_{CO_2}. This will occur once the cells are transferred to a low P_{CO_2} saline. A CO_2 insensitive gap junction will exhibit equally rapid dye transfer at low and high P_{CO_2}. *B*, images showing dye transfer between coupled cells at two different levels of P_{CO_2}. Numbers in lower right corner are recording time in minutes. Image at 0 min in both rows is a merge of differential interference contrast (DIC) and mCherry (for Cx26, red) and NBDG fluorescence (green) and is the beginning of the recording. The gap junction can be observed as a red stripe between the coupled cells (yellow arrows, both rows). Subsequent images show just the NBDG fluorescence. In 35 mmHg P_{CO_2} dye transfer to the acceptor cell is evident after 1 min (white arrows). Starting the recording at a P_{CO_2} of 55 mmHg and then transferring to 35 mmHg saline after 2 min greatly slows dye transfer; fluorescence in the acceptor cell is only seen after 10 min (white arrows). Scale bar is 20 μm. *C*, summary data for stably expressing (mouse Cx26, $n = 9$ and 18 for low and high CO_2, respectively) and transiently transfected (human Cx26 tagged with mCherry, $n = 12$ for low and high CO_2) HeLa cells, showing the time for dye in the acceptor cell to reach 10% of the donor starting in 35 mmHg, and starting in 55 mmHg but transferring to 35 mmHg after 2 min. When the recordings are commenced in 55 mmHg the dye transfer time is much longer. Statistical comparisons with Mann–Whitney *U* test.

Results

Rate of dye transfer between coupled cells shows CO_2 dependence of Cx26 gap junctions

Many investigators have used dye transfer assays to demonstrate the presence of gap junctions (Spray *et al.* 1991; Elfgang *et al.* 1995; Abbaci *et al.* 2007). We therefore adapted this type of assay to test whether increases in P_{CO_2} could alter the permeation of a fluorescent glucose analogue (NBDG) through Cx26 gap junctions formed between HeLa cells. Starting with HeLa cells that stably expressed untagged Cx26, we made whole cell recordings from a single cell in a coupled pair. After introducing NBDG, via the patch pipette, into one of the cells (the *donor*) of a coupled pair, we recorded the time taken for the dye to diffuse into the coupled (*acceptor*) cell and achieve 10% of the fluorescence intensity of the donor cell (Fig. 1*A*). If the gap junction is sensitive to CO_2, then permeation of NBDG from the donor to acceptor cell should be altered by elevated P_{CO_2} (Fig. 1*A*). By recording from pairs of HeLa cells that stably expressed Cx26, we found that NBDG rapidly permeated into coupled cells in solutions with a P_{CO_2} of 35 mmHg (Fig. 1*C*). When the recording was initiated in a saline with a P_{CO_2} of 55 mmHg, there was little permeation during the period of high P_{CO_2} and this only occurred once the P_{CO_2} was reduced to 35 mmHg (Fig. 1*C*). We refined this assay by performing it on cells that had been transiently transfected with Cx26 tagged with mCherry. This allowed us to directly visualize the gap junctions and thus select pairs of coupled cells for the assay (Fig. 1*B*). Once again, we found that the level of P_{CO_2} altered the time it took for NBDG to permeate from the donor to the acceptor cell (Fig. 1*B* and *C*).

Having established the validity of the fluorescence assay to detect CO_2-sensitive intercellular coupling, we next investigated whether the CO_2 sensitivity of Cx26 gap junctions depended on the same residues (K125 and R104) that are necessary for the CO_2 sensitivity of the Cx26 hemichannel (Meigh *et al.* 2013). We examined the effect of two mutations K125R and R104A that individually remove CO_2 sensitivity from the hemichannel. $Cx26^{K125R}$ and $Cx26^{R104A}$ formed gap junctions between HeLa cells (Fig. 2*A*) that were readily permeated by NBDG. Our data showed that unlike wild-type Cx26 gap junctions, CO_2 made no difference to the rate of dye transfer between cells coupled via $Cx26^{K125R}$ or $Cx26^{R104A}$ (Fig. 2*A* and *B*).

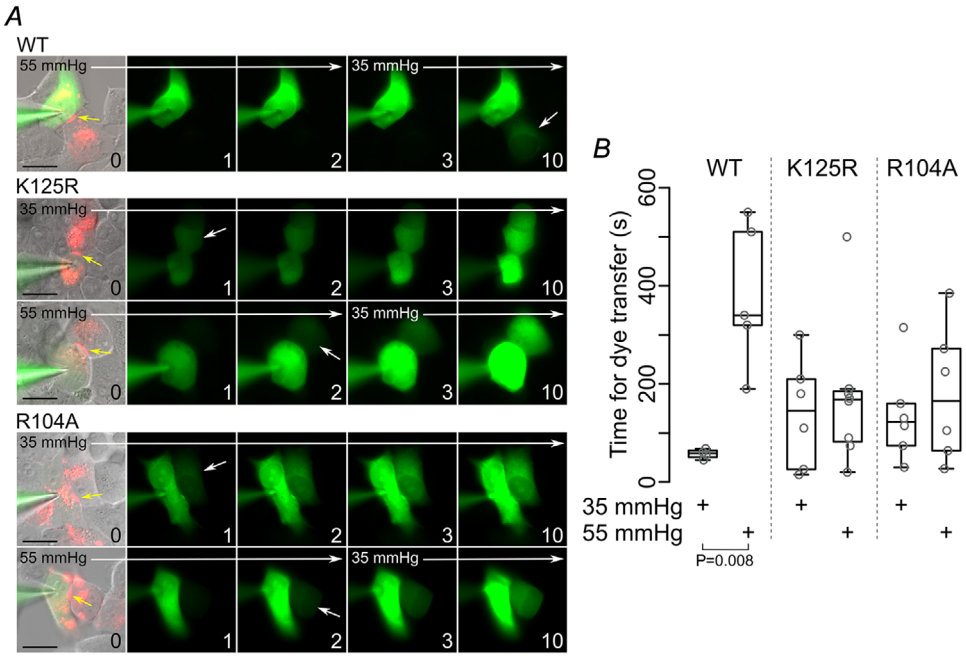

Figure 2. CO_2 dependence of Cx26 gap junction closing depends on the carbamylation motif
A, images showing permeation of NBDG through $Cx26^{WT}$, $Cx26^{K125R}$ or $Cx26^{R104A}$ at different levels of P_{CO_2}. Unlike the $Cx26^{WT}$, where elevated P_{CO_2} slows permeation of NBDG to the coupled cell, permeation of NBDG between cells coupled by $Cx26^{K125R}$ or $Cx26^{R104A}$ is apparently unaffected by P_{CO_2}. White arrows indicate appearance of NBDG in the coupled cell, yellow arrows highlight the gap junction structure; scale bar: 20 μm; numbers in bottom right corners indicate time of image in minutes after start of recording. *B*, summary data showing that rat $Cx26^{WT}$ gap junctions ($n = 4$, 35 mmHg and $n = 5$, 55 mmHg) are CO_2 sensitive (55 mmHg P_{CO_2} delays the passage of dye across the gap junction), but those comprising rat $Cx26^{K125R}$ ($n = 6$, 35 mmHg and $n = 8$, 55 mmHg) or rat $Cx26^{R104A}$ ($n = 6$, 35 and 55 mmHg) show no CO_2-dependence in the time required for dye transfer from the donor to acceptor cell. Kruskal–Wallis test $\chi^2 = 12.26$, df $= 5$, $p = 0.031$; Mann–Whitney *U* test WT 35 mmHg *vs*. WT 55 mmHg, $p = 0.008$.

CO_2-dependent gap junction closure appears to require the same residues that are essential for hemichannel opening.

Electrical coupling via Cx26 gap junctions is sensitive to CO_2

To confirm the observations made during intercellular dye transfer assays, we made simultaneous whole cell recordings from isolated pairs of Cx26-expressing HeLa cells that were in close apposition, as these cells had a high probability of being electrically coupled. On establishing whole cell recordings from each cell, the cells were clamped at a holding potential of −50 mV. We used a simple protocol of repeated 10 mV steps, alternating in each cell (see Methods). In all the illustrations, the downward currents during the voltage steps are proportional to the junctional conductance. Untransfected parental HeLa cells sometimes exhibited gap junction coupling but this was insensitive to CO_2 (median change in conductance −0.03 nS (95% CI, −0.1 to 0.11), n = 10; percentage change shown in Fig. 3*A* and *B*; absolute conductances given in Table 1). In cells that stably expressed mouse Cx26, application of hypercapnic saline (P_{CO_2} 55 mmHg) at a constant extracellular pH of 7.5 caused a reduction of junctional coupling (Fig. 3*A* and *B*, Table 1). In some cases, this was a partial effect and in other cases the coupling between cells was completely abolished. Overall the median change of the gap junction conductance (from control to 55 mmHg P_{CO_2}) was −5.6 nS (95% CI, −11.9 to −3.2 nS) (n = 29). The junctional current had a linear current voltage relation and reversed around 0 mV, as would be expected from identical recording solutions used for each cell of the coupled pair (Fig. 4, n = 3).

We next tested the requirement for the carbamylation motif for gap junction closure by CO_2 in the electrophysiological assay. Gap junctions formed between HeLa cells stably expressing $Cx26^{K125R}$ tagged with mCherry were insensitive to a P_{CO_2} of 55 mmHg (Figs 3*A* and *B*; median change in conductance 0.01 nS (95% CI, −0.06 to 0.2 nS), n = 14, Table 1). Furthermore, gap junctions of Cx31 (stably transfected into HeLa cells and tagged with mCherry), which lacks the carbamylation motif (Meigh *et al.* 2013), were also insensitive to a P_{CO_2} of 55 mmHg (Fig. 3*A* and *B*; median change in conductance 0.07 nS (95% CI, −0.29 to 0.44 nS), n = 12, Table 1).

We have therefore used two independent methods to demonstrate that Cx26 gap junctions are closed by

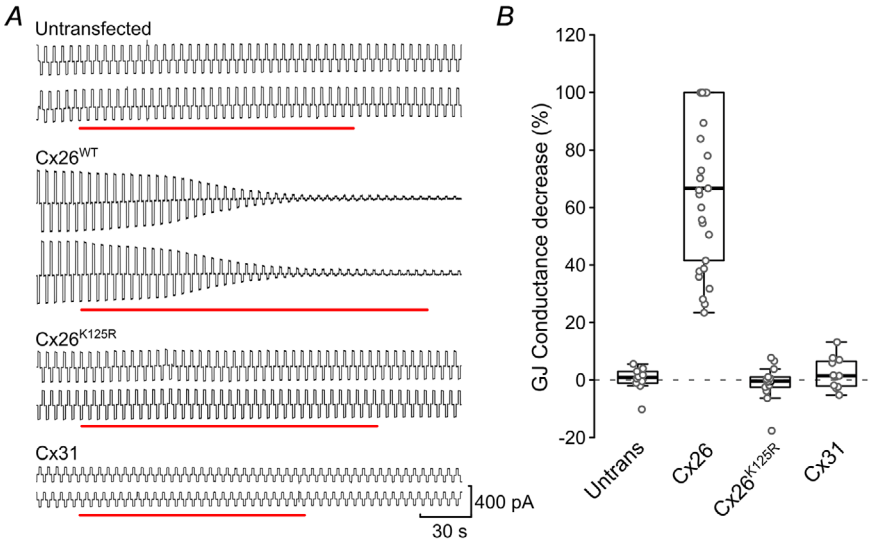

Figure 3. Cx26 gap junctions are closed by a modest increase in P_{CO_2}
A, representative examples of electrophysiological recordings from cells displaying gap junction coupling. In each case, both cells were voltage clamped at −50 mV. On top of the holding potential, alternating +10 mV (1.25 s in duration) steps were applied to each cell. The upward currents represent the whole cell current, which will include the gap junction current; the downward currents represent current flow from the cell at −40 mV to the cell at −50 mV and is thus current flow through the gap junction. Untransfected HeLa cells can exhibit coupling, but this is not sensitive to CO_2. Gap junctions formed between HeLa cells stably expressing mouse $Cx26^{WT}$ are rapidly and completely blocked by CO_2. Gap junctions formed by rat $Cx26^{K125R}$ are unaffected by CO_2, as are rat Cx31 gap junctions. Bars represent the application of saline with 55 mmHg P_{CO_2}. *B*, summary data showing the percentage decrease caused by CO_2 on gap junction coupling between untransfected (parental) HeLa cells (n = 10), and HeLa cells expressing $Cx26^{WT}$ (n = 29), $Cx26^{K125R}$ (n = 14) or Cx31 (n = 12). Kruskal–Wallis test: χ^2 = 48.1, df = 3, $p = 2 \times 10^{-10}$.

Table 1. Conductance values for gap junctions present in parental HeLa cells and HeLa cells expressing Cx31, $Cx26^{WT}$ and $Cx26^{K125R}$ at control (35 mmHg) and elevated levels of P_{CO_2}

	Gap junction conductance (ns)		
	35 mmHg	55 mmHg	% reduction
HeLa parental ($n = 10$)	15.3 (8.2–25.9)	15.5 (7.7–25.8)	0.81 (−2.1 to 3.9)
Cx31 ($n = 12$)	6.8 (3.9–10.5)	6.5 (4.1–10.4)	1.4 (−2.5 to 6.9)
$Cx26^{K125R}$ ($n = 14$)	20.0 (14.2–27.6)	19.7 (14.3–27.8)	−0.5 (−3.9 to 3.8)
$Cx26^{WT}$ ($n = 29$)	11.8 (5.3–16.1)	1.8 (0.0–5.0)	66.7 (50.5 to 100.0)

The values are presented as the median (95% CI).

moderate changes in CO_2 (a P_{CO_2} of 55 mmHg) and this CO_2-dependent closure depends upon the same residues (K125 and R104) that are required for hemichannel opening by CO_2.

CO_2-dependent and pH-dependent closure of Cx26 gap junctions can be dissociated by the K125R mutation

A possible mechanism by which CO_2 could close the gap junction is via intracellular acidification. CO_2 is known to permeate membranes and, by combining with water, can acidify the intracellular milieu. In prior studies, very high levels of CO_2 (30–100%) have been used as a pharmacological method to close a variety of gap junctions (Spray *et al.* 1991; Young & Peracchia, 2004). We therefore tested whether intracellular acidification, imposed independently of CO_2 by application of 30 mM propionate (Jahromi *et al.* 2002; Haussig *et al.* 2008), could close the Cx26 gap junction, and whether this could be altered by the K125R mutation, which eliminates CO_2-dependent closure. This level of propionic acid will cause far greater intracellular acidification than that caused by the elevated CO_2 used in this study (Cook *et al.* 2012). Propionic acid treatment reduced the gap junction conductance of wild-type Cx26 by a median of 5.3 nS (95% CI, 2.8–8.3 nS), $n = 12$, Fig. 5). This represents a median reduction of 41.7% (95% CI, 26.6–53.7%). Propionate (30 mM) also reduced the gap junction conductance of $Cx26^{K125R}$ by a similar amount: median 7.7 nS (95% CI, 4.1–11.0 nS), $n = 13$, Fig. 5). This represents a median reduction of 48.1% (95% CI, 28.0–86.3%). The actions of CO_2 and intracellular pH on the Cx26 gap junction conductance are thus of similar magnitude, but mechanistically independent. Specifically, pH-induced gap junction closure does not require K125, whereas CO_2-dependent closure does require this residue. This in turn suggests that CO_2 has a direct action on Cx26, most probably via the carbamylation reaction that we have proposed for the opening of hemichannels (Meigh *et al.* 2013), to cause closing of the gap junction.

Effect of KID syndrome mutations on CO_2-dependence of gap junction coupling

We have previously shown that KID syndrome mutations A88V, N14K and A40V (Fig. 6) abolish the ability of CO_2 to open the mutant hemichannels (Meigh *et al.* 2014; de Wolf *et al.* 2016; Cook *et al.* 2019). Recently, we discovered that certain KID syndrome mutations induce alternative splicing of the Cx26 mutation when this is tagged with a fluorescent protein (Cook *et al.* 2019). This splicing results in poor expression and cell death but can be prevented by also mutating the 5′ splice site (Cook *et al.* 2019). However, the 5′ splice site cannot be silently mutated, so we chose a conservative mutation, M151L (Fig. 6), which appeared to have little effect on Cx26 expression by itself. $Cx26^{M151L}$ hemichannels are blocked normally by extracellular Ca^{2+} and they retain CO_2 sensitivity (Cook *et al.* 2019). Furthermore, $Cx26^{A40V,M151L}$ hemichannels are insensitive to CO_2 (Cook *et al.* 2019).

When the M151L mutation was combined with the KIDS mutations, A40V, A88V or N14K (Fig. 6), in each case, the doubly mutated Cx26 was invariably capable of forming functional gap junctions through which NBDG could permeate (Fig. 7). For all three mutations, the Cx26 gap junction remained open in the presence of 55 mmHg P_{CO_2} (Fig. 7), a concentration that would normally close the wild-type gap junction (Figs 1–3). Thus, the KIDS mutations, when combined with M151L, not only prevent CO_2-dependent opening of the hemichannel, but also prevent CO_2-dependent closing of the gap junction. Interestingly, the effect of N14K on hemichannel sensitivity to CO_2 is less than those of the other KIDS mutations (de Wolf *et al.* 2016) and this parallels the trend in our data that permeation of NBDG through the $Cx26^{N14K,M151L}$ gap junctions, while still occurring, may be slightly slowed at the higher level of P_{CO_2} (Fig. 7*C* and *D*).

As the mutation M151L is a rare allele associated with non-syndromic hearing loss (Siemering *et al.* 2006), we tested whether this mutation by itself affected gap junctions. $Cx26^{M151L}$ permitted gap junction formation as gap junction plaques were clearly visible between expressing cells (Fig. 8*A*). However, in 47 different recordings we did not observe either dye coupling (Fig. 8*B*)

or the electrophysiological hallmarks of electrical coupling (slowed capacitive charging currents during a voltage step indicative of current flow through the gap junction). By contrast, cells expressing $Cx26^{A40V,M151L}$, $Cx26^{A88V,M151L}$ and $Cx26^{N14K,M151L}$ exhibited dye coupling in 14/15, 12/12 and 12/12 recordings respectively. These frequencies of coupling are statistically different $\chi^2 = 82.2$ (3 degrees of freedom, $p = 5.1 \times 10^{-18}$). We conclude that the mutation M151L prevents permeation through gap junctions that are apparently formed but either remain closed at the transjunctional potential studied here or are otherwise non-functional. This finding further implies that the KIDS mutations appear to compensate for the deficiency in gap junction permeability introduced by the M151L mutation.

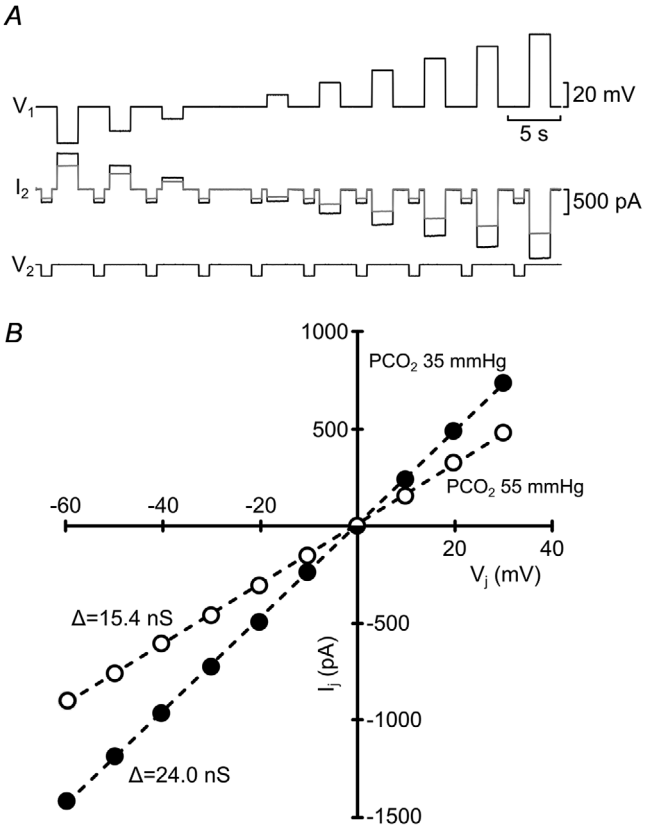

Figure 4. Junctional current through Cx26 is linear and reduced by CO_2 at all transjunctional voltages
A, raw current and voltage traces. A series of voltage steps from −80 to +10 mV in 10 mV steps were applied to cell 1 (V_1). The resulting currents were observed in cell 2 (I_2). Both cells were held at a holding potential of −50 mV. The current in cell 2 during the voltage steps in cell 1 represents the junctional current. Cell 2 also had periodic −10 mV steps to measure its whole cell conductance. A P_{CO_2} of 55 mmHg reduced the junctional currents (grey line) compared to the control (35 mmHg, black line). The whole cell conductance of cell 2 was also reduced in proportion to the reduction of the gap junction conductance by elevated P_{CO_2} (indicated by inward currents during regular −10 mV steps, V_2). This reduction in whole cell conductance occurs because the gap junction represents a resistance pathway out of the cell. *B*, plot of junctional current (I_j) *versus* transjunctional voltage (V_j) demonstrating a linear relation and the change in slope due to the action of CO_2 reducing the gap junction coupling.

Elastic network modelling

Previous experimental data point to the importance of carbamylation of K125 and the formation of a salt bridge to R104 in the adjacent subunit to facilitate Cx26 hemichannel opening in response to CO_2. It is not clear from this mechanism alone why the dodecameric Cx26 gap junction would be closed by CO_2. Previous work has used coarse-grained modelling to demonstrate a mechanism whereby CO_2 constrains the Cx26 hemichannel in the open state (Meigh *et al.* 2013). We therefore used further coarse-grained modelling to probe the difference in behaviour of the Cx26 hemichannel and gap junction. Coarse-grained modelling reduces protein atomistic complexity for efficient computational studies of harmonic protein dynamics and is particularly suited to examining the contribution of entropy to channel opening over millisecond time scales (Sherwood *et al.* 2008). While it is not possible to be certain that such calculated dynamics are true in the absence of experimentally determined structures, coarse-grained modelling has helped to support and explain structural data for membrane protein conformational changes (Shrivastava & Bahar, 2006; Sherwood *et al.* 2008; Zheng & Auerbach, 2011; Isin *et al.* 2012).

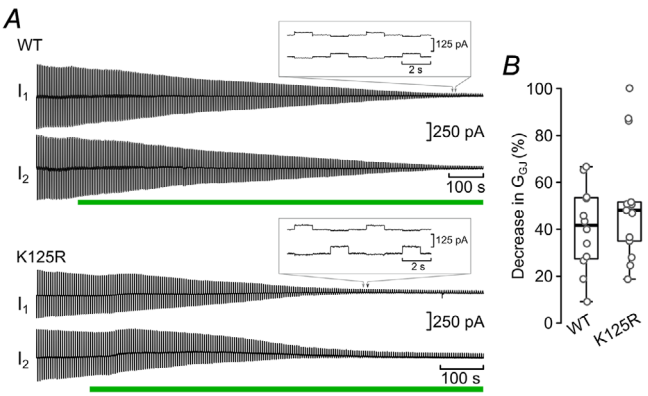

Figure 5. Intracellular acidification closes Cx26 gap junctions and is independent of the carbamylation motif
A, sample recordings of gap junctions formed between cells transiently expressing human $Cx26^{WT}$ or human $Cx26^{K125R}$ tagged with mCherry. Alternating +10 mV steps were applied to each cell; the downward currents represent the flow of current through the gap junction to the coupled cell. Application of 30 mM propionate (bar) caused a reduction in the gap junction currents, which was similar for $Cx26^{WT}$ and $Cx26^{K125R}$. The insets show the current traces at indicated time when gap junction blockade was almost complete. *B*, summary data showing the gap junction conductance decrease (%) caused by acidification of HeLa cells expressing $Cx26^{WT}$ ($n = 12$) or $Cx26^{K125R}$ ($n = 13$).

In an elastic network model (ENM) the Cα-atom coordinates of an atomic resolution structure are used to represent a protein structure. Global protein harmonic motions within the ENM consist of a defined number of modes, each of a characteristic frequency and representing a particular harmonic motion within the protein. ENMs reproduce protein global low frequency modes well in comparison to experimental data (Delarue &

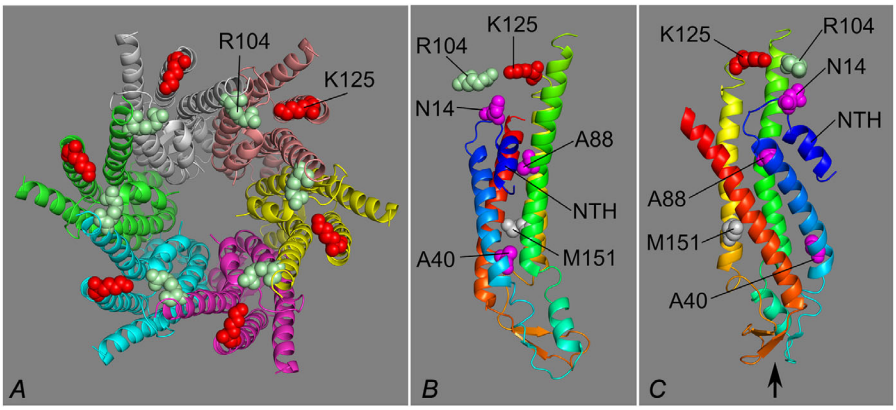

Figure 6. Position of the Cx26 carbamylation motif relative to the KIDS residues mutated in this study
A, view of the hemichannel as seen from the cytoplasmic face. Residues K125 and R104 of the carbamylation motif are shown in red and light green respectively. *B*, side view of a single subunit showing the positions of mutated residues (N14, A40 and A88 are mutated in KIDS; M151 was mutated to prevent alternative splicing of KIDS mutated mRNA). R104 from the adjacent subunit is shown aligned to K125 of the subunit. NTH: N terminal helix. *C*, additional view of the subunit after rotating it approximately 90° counterclockwise. Arrow indicates the loops in the subunit that dock to a hexamer in an opposed membrane to form a gap junction. Structure based on 2zw3 from the Protein Database.

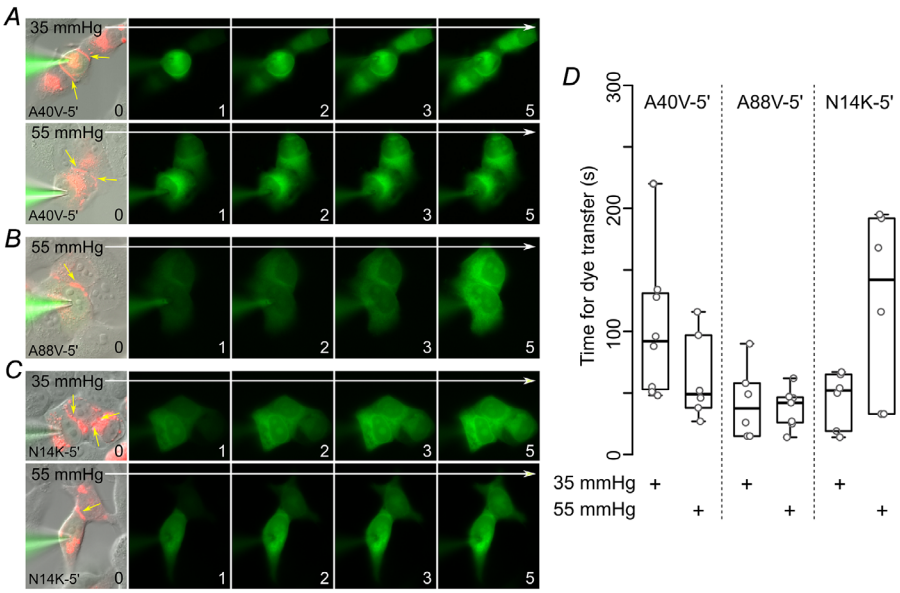

Figure 7. KIDS mutations of human Cx26 alter the CO_2 sensitivity of Cx26 gap junctions
A, gap junctions (indicated by yellow arrows) formed by $Cx26^{A40V-5'}$ (combining the A40V mutation with M151L, to eliminate alternative splicing) are highly permeable to NBDG and lack any CO_2 sensitivity. The images encompass 5 min of recording at a P_{CO_2} of 35 mmHg (top) and 55 mmHg (bottom). Permeation of NBDG to the coupled cells happens within 2 min in both conditions. *B*, gap junctions (indicated by yellow arrows) formed by $Cx26^{A88V-5'}$ are insensitive to P_{CO_2} – rapid permeation occurs to the coupled cell even at a P_{CO_2} of 55 mmHg. *C*, gap junctions formed by $Cx26^{N14K-5'}$ are not closed by CO_2. Permeation of NBDG to coupled cells is shown at P_{CO_2} of 35 mmHg (top row) and 55 mmHg (bottom row). *D*, summary data showing the time for dye transfer to the coupled cell. While A40V-5′ (n = 8, 35 mmHg; n = 6 55 mmHg) and A88V-5′ (n = 6, 35 mmHg; n = 7 55 mmHg) show no difference in permeation time with P_{CO_2}, there is a tendency for the dye to permeate more slowly to the coupled cells for N14K-5′ (n = 6 for both 35 and 55 mmHg).

Sanejouand, 2002; Valadie *et al.* 2003). We therefore built coarse-grained ENMs (Tirion, 1996) to gain insight into the mechanism by which CO_2 maintains the Cx26 hemichannel in the open state but the Cx26 gap junction in the closed state. ENMs were constructed using the coordinates from high-resolution crystal structures for the Cx26 hemichannel and gap junction in the CO_2 unbound state. CO_2 was represented in the ENMs by the inclusion of additional Hookean springs between residues K125 and R104 of neighbouring monomers in both the hemichannel and the gap junction (Meigh *et al.* 2013).

We examined the similarities between eigenvectors for the Cx26 hemichannel and gap junction to understand the changes in harmonic protein motion caused by CO_2 binding. The main open–close mode in the Cx26 hemichannel is defined as the lowest frequency mode that ignores the solid body translational and rotational motions. The solid body translational and rotational motions consist of six modes and so the open–close mode is mode 7 (Meigh *et al.* 2013). This open–close mode in the hemichannel in the absence of CO_2 (mode 7) becomes reordered as mode 15 in the presence of CO_2 (Fig. 9*A*; red-bordered square). The main open–close mode in the gap junction in the absence of CO_2 (mode 10; modes 7–9 represent motions between the two hexamer rings) becomes reordered as mode 24 in the presence of CO_2 (Fig. 9*B*; green-bordered square). Analysis of the overlap between the main open–close mode in the gap junction and hemichannel in the absence of CO_2 reveals an almost complete overlap between mode of the hemichannel (mode 7) and the gap junction (mode 10) (Fig. 9*C*, blue-bordered square). The basic open–close dynamics are therefore likely similar between gap junction and hemichannel.

To understand the differing roles of CO_2 in the hemichannel and gap junction, we calculated a range of partially open and closed eigenvectors for both the hemichannel and the gap junction. We then calculated at each state, for both the hemichannel and gap junction, the free energy for CO_2 binding and the influence of CO_2 on the open/close eigenvector. This calculation provides a free energy for each state examined along the open/close eigenvector. Calculation of the free energy difference between the CO_2-bound and -unbound state provides information on the stability (binding energy of CO_2 needed) for each state. In this case, the closer the value is to zero, the less energy is needed to bind CO_2 (Fig. 9*D*). The *x*-axis of the figure represents trajectory along the open/close eigenvector where the higher the value the more closed the hemichannel or gap junction. The *y*-axis of the figure represents the difference in free energy for the CO_2-bound and non-bound state where the higher the value is hypothesized to be less preferable for CO_2 binding. On binding CO_2, the hemichannel (6mer) or gap junction (12mer) will progress along the open/close eigenvector to make the difference in free energy more favourable for the CO_2-bound state.

For the hemichannel, it is energetically favourable to bind CO_2 in the open-state and then energetically unfavourable to close. For the gap junction it is energetically favourable to bind CO_2 in the closed state and then energetically unfavourable to open. The differences in the open/closed state of the gap junction and hemichannel in response to CO_2 can therefore be explained through entropy contributions to free energy change.

Discussion

The key result from our study is that Cx26 gap junctions are closed by a direct action of CO_2 on the protein. Our prior publications have demonstrated the opening action of CO_2 on Cx26 hemichannels (Huckstepp *et al.* 2010*a*; Meigh *et al.* 2013, 2014; de Wolf *et al.* 2016, 2017; Cook *et al.* 2019; Dospinescu *et al.* 2019). This paper further shows that these diametrically opposite actions of CO_2

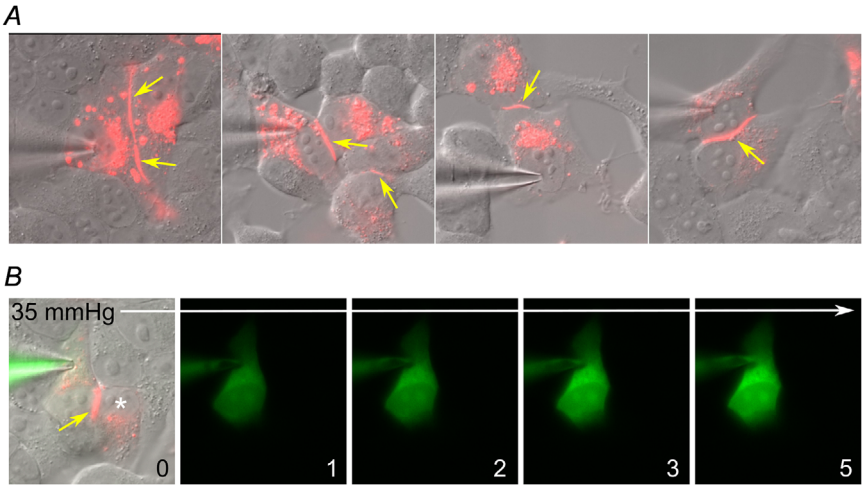

Figure 8. Physical gap junction plaques form between HeLa cells expressing human Cx26^{M151L} tagged with mCherry, but are non-functional
A, the gap junction plaques between cells are indicated by the yellow arrows. For clarity, the green channel (NBDG) has not been merged with the mCherry and DIC images. *B*, images of a cell loaded with NBDG that formed a gap junction plaque (yellow arrow) with a neighbouring cell (∗). However, NBDG does not permeate to the neighbouring cell within 5 min even at a permissive level of P_{CO_2} (35 mmHg). Numbers represent minutes from start of recording.

on gap junctions and hemichannels depend on the same residues and presumably the same carbamate bridging mechanism.

Opposing modulation of gap junctions and hemichannels has been reported before. Lipopolysaccharide and basic fibroblast growth factor inhibit Cx43 gap junctions and open Cx43 hemichannels. While apparently similar to the results reported in this study, the modulation of these two entities is downstream of kinase activity and the signalling actions of arachidonate metabolites; i.e. these are indirect effects on Cx43 and are unlikely to involve the same residues in the protein (De Vuyst *et al.* 2007). Similarly, the cytokines interleukin 1β and tumour necrosis factor α also inhibit Cx43 gap junctions and open Cx43 hemichannels (Retamal *et al.* 2007*a*). Both of these effects are mediated through a p38 mitogen-activated protein kinase (MAPK)-dependent pathway. However, hemichannel opening triggered by these cytokines is sensitive to inhibition of nitric oxide synthase or changing redox state (Retamal *et al.* 2007*b*), whereas the gap junction closure is insensitive to redox state. Thus, for the two entities, the mechanisms of modulation evoked by the p38 MAPK pathway differ (Retamal *et al.* 2007*a*).

Independence of pH- and CO_2-dependent modulation of Cx26 gap junctions

A possible alternative interpretation of our data is that CO_2 caused intracellular acidification and thus closed

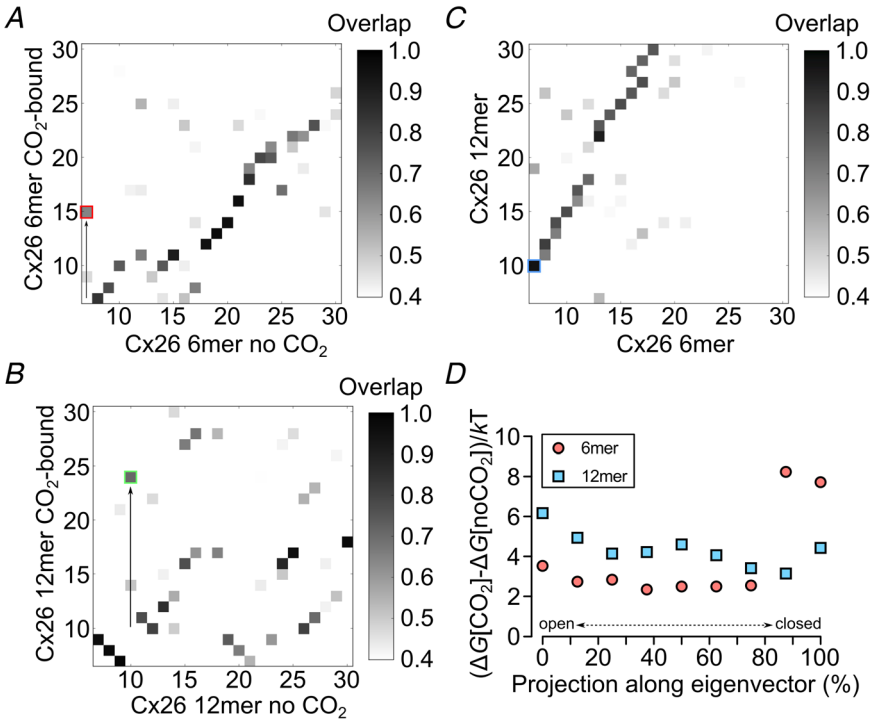

Figure 9. Analysis of the effect of CO_2 on Cx26 hemichannel and gap junction gating via elastic network modelling
A, the main open–close mode in the hemichannel (6mer) in the absence of CO_2 (mode 7) is reordered to mode 15 (red square) in the presence of CO_2. Therefore, this mode contributes less to the total motion of the molecule in the presence of CO_2 – the hemichannel spends more time open (Meigh *et al.* 2013). *B*, the main open–close mode in the gap junction (12mer) in the absence of CO_2 (mode 10) is reordered to mode 24 (green square) in the presence of CO_2. CO_2 thus reduces the contribution of this mode to the total motion of the molecule, but it is not possible to state whether the gap junction is predominantly in the closed or open state from this analysis alone. *C*, correspondence of the modes for the hemichannel (6 mer) and gap junction (12 mer). Mode 7 in the hemichannel corresponds very closely to mode 10 in the gap junction (indicated by blue square). *D*, for a range of partially open and closed eigenvectors for both the hemichannel and the gap junction, we then calculated the change in free energy on CO_2 binding and thus the influence of CO_2 on the open/closed eigenvector. The closer the free energy value is to zero, the less energy is needed to bind CO_2. The *x*-axis represents trajectory along the open/closed eigenvector going from fully open to fully closed. The *y*-axis represents the free energy for binding CO_2 where the higher the value the less preferable is CO_2 binding. For the hemichannel, CO_2 binding is less energetically favourable in the closed state, whereas for the gap junction CO_2 binding is favoured in the closed state.

the gap junction. Under this interpretation, CO_2 would have no direct action on Cx26. This interpretation is unlikely for two reasons. Firstly, only modest increases in P_{CO_2} around the physiological norm were required to close Cx26 gap junctions. Such changes will only cause modest intracellular acidification. By contrast very profound acidification to pH values below 6.5 is required to close the Cx26 gap junction channel (Khan *et al.* 2020). Secondly, and more importantly, the mutation K125R prevents the CO_2-dependent closure of the gap junction, but does not affect the closing effect of acidification induced by application of propionate (Fig. 4). The actions of CO_2 and pH on the gap junction are therefore mechanistically independent at the moderate levels of CO_2 used in this study. This independence of mechanistic action of pH and CO_2 is also true for Cx26 hemichannels as acidification causes hemichannel closure (Yu *et al.* 2007), whereas a modest increase in P_{CO_2} causes hemichannel opening (Huckstepp *et al.* 2010*a*; Meigh *et al.* 2013; de Wolf *et al.* 2017; Cook *et al.* 2019; Hill *et al.* 2020).

Although the carbamylation motif in Cx26 is required for both the CO_2-dependent opening of hemichannels and the CO_2-dependent closure of gap junctions, the link between the CO_2-dependent modulation of hemichannels and gap junctions is not immutable. Cx26 hemichannels of the lungfish *Lepidosiren* are insensitive to CO_2 owing to the presence of an extended C-terminus, yet their gap junctions are still closed by CO_2 (Dospinescu *et al.* 2019). The contrary case is demonstrated by Cx32: hemichannels of this connexin can be opened by CO_2, but Cx32 gap junctions are insensitive to the same doses of CO_2 (Dospinescu *et al.* 2019).

Implications for structural biology of Cx26

The crystal structure of Cx26 shows the molecule in the form of a gap junction (Maeda *et al.* 2009). The two connexons dock via interactions involving the two extracellular loops (E1 and E2) of each subunit. There are multiple hydrogen bonds formed between the opposing E1 and E2 loops of each connexon (Maeda *et al.* 2009). These give a tight interaction that is likely to alter and constrain the conformation of hemichannels docked in a gap junction *versus* undocked hemichannels. The opposing modulation of gap junctions and hemichannels by CO_2 must presumably arise from the conformational differences between free *versus* docked hemichannels.

Our ENM calculations of the interaction of CO_2 with Cx26 hemichannels used the docked hemichannel from the gap junction as a model for the structure of the free hemichannel (Meigh *et al.* 2013). This model allowed us to propose a plausible gating mechanism for CO_2-dependent opening of the hemichannel, which we have supported with extensive mutational analysis (Meigh *et al.* 2013). We exploited this knowledge to introduce novel gating mechanisms via the same intersubunit interactions by mutating Lys125 to Cys (Meigh *et al.* 2015). This made the hemichannel NO-sensitive, via nitrosylation of the Cys125 and interaction with Arg104 of the neighbouring subunit. The double mutation K125C–R104C made the hemichannel redox sensitive (via redox modulation of disulfide bridges between subunits) (Meigh *et al.* 2015). The mutated residues in these Cx26 variants are some considerable distance apart – far further than the short distances normally required for the ionic and covalent interactions between the respective residues. That these mutations were nevertheless effective at changing the gating of Cx26 implies considerable flexibility of the hemichannel that can bring apparently distant residues close enough to interact (Meigh *et al.* 2015).

Despite this success in using a half gap junction as a model for the free hemichannel, the results in this study suggest the need for considerable caution in any future structural modelling of hemichannels. Not only may the isolated hemichannel be far more flexible than a hemichannel that is part of a gap junction, but it may also have a substantially different conformation. New structures of Cx26 hemichannels and gap junctions are therefore needed to probe their conformational differences, and provide firm mechanistic understanding of the differential modulation of hemichannels and gap junctions by CO_2.

KIDS mutations and Cx26 gap junctions

There are relatively few reports of the effects of KIDS mutations on Cx26 gap junctions. Prior reports suggest that the A40V mutation prevents Cx26 gap junction formation (Montgomery *et al.* 2004). Whilst we were not able to study the KIDS mutations in isolation owing to alternative splicing of the mRNA of the mutated Cx26, we could study the effect of these mutations in combination with M151L to prevent this alternative splicing. Clearly our data suggest that, in HeLa cells and in combination with the mutation M151L, the A40V mutation does not prevent formation of functional gap junctions (Fig. 7*A*). Our data suggest further that N14K and A88V KIDS mutations (once again in combination with M151L) do not prevent gap junction formation and that these gap junctions are highly permeable to NBDG. It is possible, however, that without being combined with M151L these three KIDS mutations might by themselves prevent functional gap junction formation. However, this possibility is made less likely by the observation that in an oocyte expression system $Cx26^{A40V}$ can form functional gap junctions (Sanchez *et al.* 2010). This same expression system has also been used to demonstrate that $Cx26^{N14K}$ can form gap junctions (Lee *et al.* 2009).

KIDS mutations are thought to cause the syndrome through gain-of-function. Several lines of evidence suggest that KIDS mutated Cx26 hemichannels are leaky: either they are less sensitive to Ca^{2+} blockade (Sanchez *et al.* 2010; Mese *et al.* 2011; Lopez *et al.* 2013; Zhang & Hao, 2013; Sanchez *et al.* 2014) or have an altered voltage sensitivity such that they spend more time in the open state at transmembrane potentials closer to the resting potential (Sanchez *et al.* 2016; Valdez Capuccino *et al.* 2019). Our finding that three KIDS mutations studied here prevent gap junctions from closing to CO_2 is effectively a further gain of function caused by these mutations: they will remain open under conditions of elevated CO_2. An important caveat is that we could only study the effect of these mutations on CO_2 sensitivity in combination with M151L. It is possible that by themselves these mutations might affect CO_2 sensitivity of the gap junctions somewhat differently. Interestingly, A40V hemichannels in oocytes are less sensitive to pH blockade than wild-type Cx26 hemichannels, indicating that this mutation has multiple effects on the gating of these channels (Sanchez *et al.* 2014). It is also interesting that the three KIDS mutations tested here could compensate for the loss of gap junction coupling induced by M151L. This observation is suggestive that these mutations modify channel gating in a dominant manner and is also consistent with the gain-of-function hypothesis.

Although not a KIDS mutation, M151L has been reported to be associated with deafness (Siemering *et al.* 2006). Our finding that it prevents functional gap junction communication suggests a possible underlying mechanistic cause of hearing loss with this mutation. The endocochlear potential is essential for hearing – it provides the driving force for K^+ to enter the hair cells through the mechanosensory ion channels present in their stereocilia. Cx26 gap junctions are a pathway for diffusion of K^+ between the fibrocytes, basal cells and intermediate cells of the stria vascularis (Wangemann, 2006) and have been proposed to form part of the pathway that recycles K^+ away from the hair cells and back into the endolymph, although this has been disputed (Zhao, 2017). Genetic deletion of Cx26 reduces the endocochlear potential by about half (Chen *et al.* 2014). Given that M151L prevents gap junction coupling (although not the formation of gap junctions *per se*), we predict that it would reduce the endocochlear potential and that this is the reason for hearing impairment.

Physiological implications

As Cx26 exists both as gap junctions and hemichannels, our findings have substantial physiological significance. In the context of breathing, Cx26 hemichannels are important and we have already explored their significance for chemosensory control (Huckstepp *et al.* 2010*b*; van de Wiel *et al.* 2020). However, there are reports of gap junctions in various nuclei implicated in the control of breathing (Dean *et al.* 2002; Solomon *et al.* 2003). CO_2-dependent uncoupling of Cx26 gap junctions between cells may therefore be an additional mechanism that contributes to chemosensory control.

In lungfish and amphibia, hemichannels of Cx26 are insensitive to CO_2 despite possessing the carbamylation motif (Dospinescu *et al.* 2019). The extended C-terminal tail of Cx26 in these species interferes with hemichannel opening. However, the Cx26 gap junctions of these species can still be closed by CO_2 (Dospinescu *et al.* 2019). The ancestral function of the carbamylation motif in Cx26 was therefore most likely to close the gap junction and the new function of hemichannel opening only arose in the amniotes (Dospinescu *et al.* 2019). Given that it has been conserved over many hundreds of millions of years, the CO_2-dependent closure of Cx26 gap junctions must have some important physiological function. What this may be remains open to question, but we speculate that if a single cell in a coupled network were to be excessively metabolically active, it would act as a sink for metabolites such as ATP, glucose or lactate from the coupled cells. As the metabolically active cell would produce more CO_2 this could be a self-regulating mechanism to preserve network integrity by uncoupling the 'run-away' cell from the network thereby reducing its drain on the communal pool of metabolites. It is interesting in this context that the P_{CO_2} of renal cortex and liver (respectively 57 and 64 mmHg), two organs where Cx26 and Cx32 are abundantly expressed, is considerably higher than the P_{CO_2} of systemic circulation (39–45 mmHg) (Hogg *et al.* 1984).

References

Abbaci M, Barberi-Heyob M, Stines JR, Blondel W, Dumas D, Guillemin F & Didelon J (2007). Gap junctional intercellular communication capacity by gap-FRAP technique: a comparative study. *Biotechnol J* **2**, 50–61.

Brotherton DH, Savva C, Ragan T, Linthwaite V, Cann M, Dale N & Cameron AD (2020). Conformational changes and channel gating induced by CO_2 binding to Connexin26. *bioRxiv*, 2020.2008.2011.243964.

Chen J, Chen J, Zhu Y, Liang C & Zhao HB (2014). Deafness induced by Connexin 26 (GJB2) deficiency is not determined by endocochlear potential (EP) reduction but is associated with cochlear developmental disorders. *Biochem Biophys Res Commun* **448**, 28–32.

Cook J, de Wolf E & Dale N (2019). Cx26 keratitis ichthyosis deafness syndrome mutations trigger alternative splicing of Cx26 to prevent expression and cause toxicity in vitro. *R Soc Open Sci* **6**, 191128.

Cook ZC, Gray MA & Cann MJ (2012). Elevated carbon dioxide blunts mammalian cAMP signaling dependent on inositol 1,4,5-triphosphate receptor-mediated Ca^{2+} release. *J Biol Chem* **287**, 26291–26301.

Dean JB, Ballantyne D, Cardone DL, Erlichman JS & Solomon IC (2002). Role of gap junctions in CO_2 chemoreception and respiratory control. *Am J Physiol Lung Cell Mol Physiol* **283**, L665–L670.

Delarue M & Sanejouand YH (2002). Simplified normal mode analysis of conformational transitions in DNA-dependent polymerases: the elastic network model. *J Mol Biol* **320**, 1011–1024.

De Vuyst E, Decrock E, De Bock M, Yamasaki H, Naus CC, Evans WH & Leybaert L (2007). Connexin hemichannels and gap junction channels are differentially influenced by lipopolysaccharide and basic fibroblast growth factor. *Mol Biol Cell* **283**, L665-L670.

de Wolf E, Cook J & Dale N (2017). Evolutionary adaptation of the sensitivity of connexin26 hemichannels to CO_2. *Proc R Soc B* **284**, 20162723.

de Wolf E, van de Wiel J, Cook J & Dale N (2016). Altered CO_2 sensitivity of connexin26 mutant hemichannels in vitro. *Physiol Rep* **4**, e13038.

Dospinescu V-M, Nijjar S, Spanos F, Cook J, de Wolf E, Biscotti MA, Gerdol M & Dale N (2019). Structural determinants of CO_2-sensitivity in the β connexin family suggested by evolutionary analysis. *Commun Biol* **2**, 331.

Elfgang C, Eckert R, Lichtenberg-Fraté H, Butterweck A, Traub O, Klein RA, Hülser DF & Willecke K (1995). Specific permeability and selective formation of gap junction channels in connexin-transfected HeLa cells. *J Cell Biol* **129**, 805–817.

Haussig S, Schubert A, Mohr FW & Dhein S (2008). Sub-chronic nicotine exposure induces intercellular communication failure and differential down-regulation of connexins in cultured human endothelial cells. *Atherosclerosis* **196**, 210–218.

Hill E, Dale N & Wall MJ (2020). Moderate changes in CO_2 modulate the firing of neurons in the VTA and substantia nigra. *iScience*, **23**, 101343.

Hogg RJ, Pucacco LR, Carter NW, Laptook AR & Kokko JP (1984). In situ PCO_2 in the renal cortex, liver, muscle, and brain of the New Zealand White rabbit. *Am J Physiol* **247**, F491–F498.

Huckstepp RT & Dale N (2011). Redefining the components of central CO_2 chemosensitivity – towards a better understanding of mechanism. *J Physiol* **589**, 5561–5579.

Huckstepp RT, Eason R, Sachdev A & Dale N (2010*a*). CO_2-dependent opening of connexin 26 and related beta connexins. *J Physiol* **588**, 3921–3931.

Huckstepp RT, id Bihi R, Eason R, Spyer KM, Dicke N, Willecke K, Marina N, Gourine AV & Dale N (2010*b*). Connexin hemichannel-mediated CO_2-dependent release of ATP in the medulla oblongata contributes to central respiratory chemosensitivity. *J Physiol* **588**, 3901–3920.

Isin B, Tirupula KC, Oltvai ZN, Klein-Seetharaman J & Bahar I (2012). Identification of motions in membrane proteins by elastic network models and their experimental validation. *Methods Mol Biol* **914**, 285–317.

Jahromi SS, Wentlandt K, Piran S & Carlen PL (2002). Anticonvulsant actions of gap junctional blockers in an in vitro seizure model. *J Neurophysiol* **88**, 1893–1902.

Kang J, Kang N, Lovatt D, Torres A, Zhao Z, Lin J & Nedergaard M (2008). Connexin 43 hemichannels are permeable to ATP. *J Neurosci* **28**, 4702–4711.

Khan AK, Jagielnicki M, McIntire WE, Purdy MD, Dharmarajan V, Griffin PR & Yeager M (2020). A steric "ball-and-chain" mechanism for pH-mediated regulation of gap junction channels. *Cell Rep* **31**, 107482.

Lee JR, Derosa AM & White TW (2009). Connexin mutations causing skin disease and deafness increase hemichannel activity and cell death when expressed in *Xenopus* oocytes. *J Invest Dermatol* **129**, 870–878.

Lopez W, Gonzalez J, Liu Y, Harris AL & Contreras JE (2013). Insights on the mechanisms of Ca^{2+} regulation of connexin26 hemichannels revealed by human pathogenic mutations (D50N/Y). *J Gen Physiol* **142**, 23–35.

Lorimer GH (1983). Carbon-dioxide and carbamate formation – the makings of a biochemical control-system. *Trends Biochem Sci* **8**, 65–68.

Maeda S, Nakagawa S, Suga M, Yamashita E, Oshima A, Fujiyoshi Y & Tsukihara T (2009). Structure of the connexin 26 gap junction channel at 3.5 Å resolution. *Nature* **458**, 597–602.

Meigh L(2015). CO_2 carbamylation of proteins as a mechanism in physiology. *Biochem Soc Trans* **43**, 460–464.

Meigh L, Cook D, Zhang J & Dale N (2015). Rational design of new NO and redox sensitivity into connexin26 hemichannels. *Open Biol* **5**, 140208.

Meigh L, Greenhalgh SA, Rodgers TL, Cann MJ, Roper DI & Dale N (2013). CO_2 directly modulates connexin 26 by formation of carbamate bridges between subunits. *Elife* **2**, e01213.

Meigh L, Hussain N, Mulkey DK & Dale N (2014). Connexin26 hemichannels with a mutation that causes KID syndrome in humans lack sensitivity to CO_2. *Elife* **3**, e04249.

Mese G, Sellitto C, Li L, Wang HZ, Valiunas V, Richard G, Brink PR & White TW (2011). The Cx26-G45E mutation displays increased hemichannel activity in a mouse model of the lethal form of keratitis-ichthyosis-deafness syndrome. *Mol Biol Cell* **22**, 4776–4786.

Montgomery JR, White TW, Martin BL, Turner ML & Holland SM (2004). A novel connexin 26 gene mutation associated with features of the keratitis-ichthyosis-deafness syndrome and the follicular occlusion triad. *J Am Acad Dermatol* **51**, 377–382.

Pearson RA, Dale N, Llaudet E & Mobbs P (2005). ATP released via gap junction hemichannels from the pigment epithelium regulates neural retinal progenitor proliferation. *Neuron* **46**, 731–744.

Retamal MA, Froger N, Palacios-Prado N, Ezan P, Sáez PJ, Sáez JC & Giaume C (2007*a*). Cx43 hemichannels and gap junction channels in astrocytes are regulated oppositely by proinflammatory cytokines released from activated microglia. *J Neurosc* **27**, 13781–13792.

Retamal MA, Schalper KA, Shoji KF, Bennett MV & Saez JC (2007*b*). Opening of connexin 43 hemichannels is increased by lowering intracellular redox potential. *Proc Natl Acad Sci U S A* **104**, 8322–8327.

Rodgers TL, Burnell D, Townsend PD, Pohl E, Cann MJ, Wilson MR & McLeish TC (2013*a*). ΔΔPT: a comprehensive toolbox for the analysis of protein motion. *BMC Bioinformatics* **14**, 183.

Rodgers TL, Townsend PD, Burnell D, Jones ML, Richards SA, McLeish TC, Pohl E, Wilson MR & Cann MJ (2013*b*). Modulation of global low-frequency motions underlies allosteric regulation: demonstration in CRP/FNR family transcription factors. *PLoS Biol* **11**, e1001651.

Sanchez HA, Bienkowski R, Slavi N, Srinivas M & Verselis VK (2014). Altered inhibition of Cx26 hemichannels by pH and Zn^{2+} in the A40V mutation associated with keratitis-ichthyosis-deafness syndrome. *J Biol Chem* **289**, 21519–21532.

Sanchez HA, Mese G, Srinivas M, White TW & Verselis VK (2010). Differentially altered Ca^{2+} regulation and Ca^{2+} permeability in Cx26 hemichannels formed by the A40V and G45E mutations that cause keratitis ichthyosis deafness syndrome. *J Gen Physiol* **136**, 47–62.

Sanchez HA, Slavi N, Srinivas M & Verselis VK (2016). Syndromic deafness mutations at Asn 14 differentially alter the open stability of Cx26 hemichannels. *J Gen Physiol* **148**, 25–42.

Sherwood P, Brooks BR & Sansom MS (2008). Multiscale methods for macromolecular simulations. *Curr Opin Struct Biol* **18**, 630–640.

Shrivastava IH & Bahar I (2006). Common mechanism of pore opening shared by five different potassium channels. *Biophys J* **90**, 3929–3940.

Siemering K, Manji SS, Hutchison WM, Du Sart D, Phelan D & Dahl HH (2006). Detection of mutations in genes associated with hearing loss using a microarray-based approach. *J Mol Diagn* **8**, 483–489; quiz 528.

Solomon IC, Chon KH & Rodriguez MN (2003). Blockade of brain stem gap junctions increases phrenic burst frequency and reduces phrenic burst synchronisation in adult rat. *J Neurophysiol* **89**, 135–149.

Spray DC, Moreno AP, Kessler JA & Dermietzel R (1991). Characterization of gap junctions between cultured leptomeningeal cells. *Brain Res* **568**, 1–14.

Stout C, Goodenough DA & Paul DL (2004). Connexins: functions without junctions. *Curr Opin Cell Biol* **16**, 507–512.

Stout CE, Costantin JL, Naus CC & Charles AC (2002). Intercellular calcium signaling in astrocytes via ATP release through connexin hemichannels. *J Biol Chem* **277**, 10482–10488.

Tirion MM(1996). Large amplitude elastic motions in proteins from a single-parameter, atomic analysis. *Phys Rev Lett* **77**, 1905–1908.

Townsend PD, Rodgers TL, Pohl E, Wilson MR, McLeish TC & Cann MJ (2015). Global low-frequency motions in protein allostery: CAP as a model system. *Biophys Rev* **7**, 175–182.

Valadie H, Lacapcre JJ, Sanejouand YH & Etchebest C (2003). Dynamical properties of the MscL of *Escherichia coli*: a normal mode analysis. *J Mol Biol* **332**, 657–674.

Valdez Capuccino JM, Chatterjee P, Garcia IE, Botello-Smith WM, Zhang H, Harris AL, Luo Y & Contreras JE (2019). The connexin26 human mutation N14K disrupts cytosolic intersubunit interactions and promotes channel opening. *J Gen Physiol* **151**, 328–341.

van deWiel J, Meigh L, Bhandare A, Cook J, Nijjar S, Huckstepp R & Dale N (2020). Connexin26 mediates CO_2-dependent regulation of breathing via glial cells of the medulla oblongata. *Commun Biol* **3**, 521.

Wang HL, Chang WT, Li AH, Yeh TH, Wu CY, Chen MS & Huang PC (2003). Functional analysis of connexin-26 mutants associated with hereditary recessive deafness. *J Neurochem* **84**, 735–742.

Wangemann P (2006). Supporting sensory transduction: cochlear fluid homeostasis and the endocochlear potential. *J Physiol* **576**, 11–21.

Weissman TA, Riquelme PA, Ivic L, Flint AC & Kriegstein AR (2004). Calcium waves propagate through radial glial cells and modulate proliferation in the developing neocortex. *Neuron* **43**, 647–661.

Young KC & Peracchia C (2004). Opposite Cx32 and Cx26 voltage-gating response to CO_2 reflects opposite voltage-gating polarity. *J Membr Biol* **202**, 161–170.

Yu J, Bippes CA, Hand GM, Muller DJ & Sosinsky GE (2007). Aminosulfonate modulated pH-induced conformational changes in connexin26 hemichannels. *J Biol Chem* **282**, 8895–8904.

Zhang Y & Hao H (2013). Conserved glycine at position 45 of major cochlear connexins constitutes a vital component of the Ca^{2+} sensor for gating of gap junction hemichannels. *Biochem Biophys Res Commun* **436**, 424–429.

Zhao HB (2017). Hypothesis of K^+-recycling defect is not a primary deafness mechanism for Cx26 (GJB2) deficiency. *Front Mol Neurosci* **10**, 162.

Zheng W & Auerbach A (2011). Decrypting the sequence of structural events during the gating transition of pentameric ligand-gated ion channels based on an interpolated elastic network model. *PLoS Comput Biol* **7**, e1001046.

Additional information

Data availability statement

All data generated or analysed during this study are included in the published article in the figures and supplementary material.

Competing interests

None.

Author contributions

S.N., D.M. and N.D.: acquisition and analysis of data. L.M. and E.d.W.: generation of mutants and stable cell lines. T.R. and M.C.: elastic network modelling. N.D. wrote the paper and all authors commented on the final version. All authors have read and approved the final version of this manuscript and agree to be accountable for all aspects of the work in ensuring that questions

related to the accuracy or integrity of any part of the work are appropriately investigated and resolved. All persons designated as authors qualify for authorship, and all those who qualify for authorship are listed.

Funding

We thank the MRC (MR/P010393/1) (N.D.) and BBSRC (BB/S015132/1) (M.C.) for support. N.D. is a Royal Society Wolfson Research Merit Award Holder.

Keywords

cell coupling, connexin, gap junction, hemichannel

Supporting information

Additional supporting information may be found online in the Supporting Information section at the end of the article.

Statistical Summary Document
Raw data for Figs 1, 2, 3, 5, 7 and Table 1